International Journal of Nanomedicine

Dovepress
open access to scientific and medical research

Open Access Full Text Article

ORIGINAL RESEARCH

Dual-Drug Loaded Nanobubbles Combined with Sonodynamic and Chemotherapy for Hepatocellular Carcinoma Therapy

Tiantian Guo[1], Yao Wang[1], Dixuan Chen[2], Sifan Cui[2], Shuyue Guo[1], Yixing Feng[1], Jialin Zhu[1], Luchen Chang[1], Jiawei Zhang[2], Xiujun Gao[2], Xi Wei[1]

[1]Department of Diagnostic and Therapeutic Ultrasonography, Tianjin Medical University Cancer Institute and Hospital, National Clinical Research Center of Cancer, Key Laboratory of Cancer Prevention and Therapy, Tianjin Medical University, Tianjin, 300060, People's Republic of China; [2]School of Biomedical Engineering and Technology, Tianjin Medical University, Tianjin, 300070, People's Republic of China

Correspondence: Xi Wei, Department of Diagnostic and Therapeutic Ultrasonography, Tianjin Medical University Cancer Institute and Hospital, National Clinical Research Center for Cancer, Key Laboratory of Cancer Prevention and Therapy, Tianjin's Clinical Research Center for Cancer, Huanhuxi Road, Tiyuanbei, Hexi District, Tianjin, 300060, People's Republic of China, Email weixi@tmu.edu.cn; Xiujun Gao, School of Biomedical, Engineering and Technology, Tianjin Medical University, No. 22, Meteorological Station Road, Tianjin, 300070, People's Republic of China, Email gaoxiujun12242@tmu.edu.cn

Purpose: Chemotherapy remains the primary therapeutic approach for advanced Hepatocellular Carcinoma (HCC). The therapeutic effect of chemotherapy is limited and the toxic side effects are serious. The aim of this study is to develop a nanobubble that is ultrasonically responsive to reduce the toxic side effects of direct chemotherapy.

Methods: We developed curcumin/doxorubicin-cis-aconitic anhydride-polyethylene glycol nanobubble (C/DCNB) surface modified with acid-sensitive polyethylene glycol (PEG). And it is loaded with curcumin (CUR) and doxorubicin (DOX), as liposomes at the nanoscale for diagnosis and therapy of tumors.

Results: In this study, the acid-sensitive PEG on the surface layer of nanobubbles serves to stabilize them in the blood circulatory system and in normal tissues, while peeling off in the acidic tumor microenvironment (pH 6.8). C/DCNB can identify tumor sites through contrast-enhanced ultrasound (CEUS). And ultrasound-mediated nanobubbles promote permeability of the tumor vascular, thus improving the enhanced permeability and retention (EPR) effects in the tumor, leading to the accumulation of nanobubbles in the tumor. After endocytosis of nanobubbles, drugs are released and curcumin generates reactive oxygen species (ROS) under ultrasound conditions. CUR can enhance the sensitivity of tumor cells to DOX by inhibiting the expression of P-glycoprotein. In vitro and vivo experiments demonstrate that C/DCNB can facilitate contrast-enhanced ultrasound imaging while simultaneously delivering drugs, enabling both imaging and treatment.

Conclusion: The combination of C/DCNB and ultrasound provides an effective strategy for improving the efficiency of HCC therapy and imaging.

Keywords: combination of sonodynamic therapy and chemotherapy, the synergistic effect of two drugs, integration of diagnosis and treatment, ultrasound

Introduction

Hepatocellular Carcinoma, being one of the most common fatal malignancies, typically has a poor prognosis.[1–3] Most patients are diagnosed at an advanced or terminal stage. Advanced hepatocellular carcinoma exhibits strong resistance to chemotherapy, and traditional chemotherapy drugs often fail to achieve satisfactory therapeutic effects.[4] The complexity and heterogeneity of malignant tumors seriously undermine the efficiency of mono-modal treatment. Multi-modal nanoparticles have made remarkable progress in improving the effectiveness of chemotherapeutic drugs.[5]

Received: 23 January 2024
Accepted: 26 June 2024
Published: 19 July 2024

Graphical Abstract

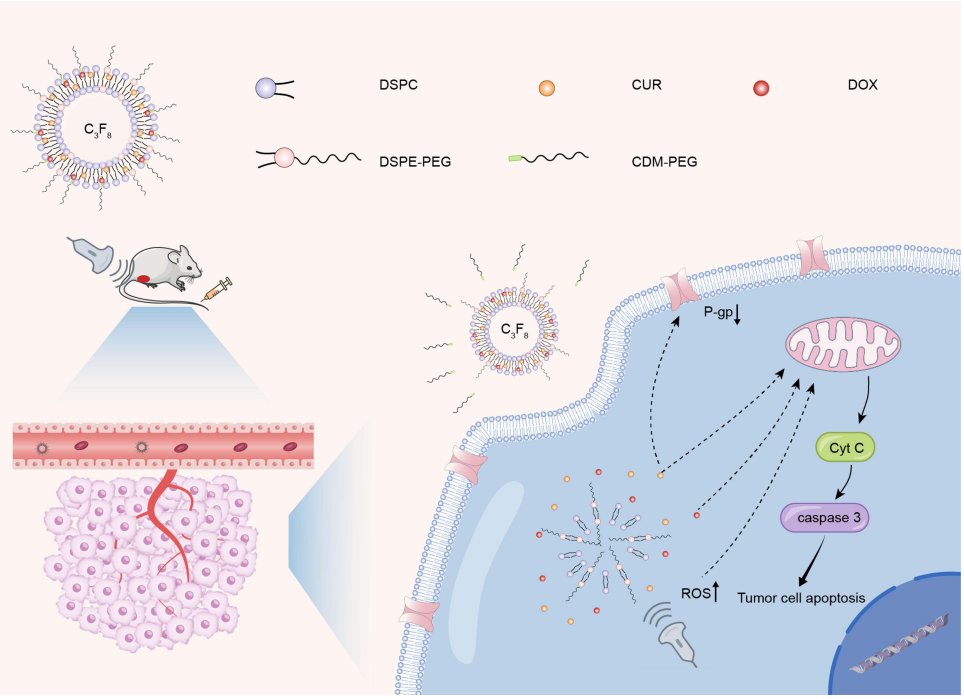

Compared with traditional chemotherapy, sonodynamic therapy (SDT) has the characteristics of non-invasiveness, low side effects and high treatment efficiency,[6] which has broad application prospects in clinical cancer treatment.[7–9] Combining sonodynamic therapy with chemotherapy can improve the efficacy of tumor therapy.[10,11] Curcumin has proved itself to be an effective sonosensitizer through generating ROS upon exposure to ultrasound.[12] As a traditional drug, DOX have been used to treat various types of cancer. However, its resistance is a major barrier to successful treatment in clinical application.[13] Curcumin can inhibit the expression of p-glycoprotein[14] to reduce the efflux of DOX, thereby reversing its resistance. However, due to the poor aqueous solubility and low bioavailability of curcumin, its clinical application is limited.[15] It is critical to develop an efficient method for site-specific delivery of drugs.

Ultrasound has the advantages of real-time observation, non-invasiveness, and high safety.[9,16,17] The contrast-enhanced ultrasound imaging has improved the resolution and sensitivity of ultrasound images, and the particle size of ultrasound contrast agent is between 1 and 10 μm.[18,19] However, microscale liposomes cannot reach the tumor microenvironment through the tumor vasculature. Nanometer-scale liposomal vesicles were designed to enable effective tumor uptake via the leaky tumor vasculature.[7] Nanobubbles exhibit greater stability than microbubbles, prolonged circulation times, and enhanced ability to passively target tumor tissue via the EPR effect. The accumulation of nanobubbles in the tumor area can lead to higher imaging quality and more effective drug delivery.[20,21] At the same time, nanobubbles have also been widely operated as carriers for loading different drugs,[22,23] achieving the combination of tumor treatment and imaging.

In this study, C/DCNB loaded with CUR and DOX were constructed and surface modified with cis-aconitic anhydride-polyethylene glycol (CDM-PEG). The interior of C/DCNB was filled with perfluoropropane (C_3F_8). The C/DCNB can be imaged by contrast-enhanced ultrasound to identify the tumor, shed the PEG after reaching the acidic tumor microenvironment.[24–26] And ultrasound in combination with nanobubbles promotes the further accumulation at the tumor site. After being internalized into cells, SDT and chemotherapeutic exhibit synergistic anti-tumor activities in vitro and vivo, which has a great potential in improving the efficiency of the therapy of HCC.

Materials and Methods

Materials

1, 2-distearoyl-Sn-glycerol-3-pHospHocholine (DSPC) was purchased from XIAMEN SINOPEG BIOTECH CO., LTD., China. 1.2-distearoyl-sn-glycero-3-phosphoethanolamine-N-[methoxy(polyethylene glycol)] (DSPE-PEG) was purchased from Tanshui Technology Co., Ltd., China. Doxorubicin, curcumin, Rhodamine B, 4% paraformaldehyde, deuterated water (D_2O), deuterated dimethyl sulfoxide (DMSO-D_6), deuterated chloroform (Chloroform-D), anhydrous ethanol, tetrahydrofuran, anhydrous formaldehyde, N,N-Dimethylformamide (DMF, anhydrous), 2.5-dihydro-2,5-dioxofuran-3-acetic acid (CDM), 4-dimethylaminopyridine (DMAP) were purchased from Ponsure Biotechnology Co., Ltd. (Shanghai, China), Western blot antibody was purchased from Sunon Biotechnology Co., LTD. (Shanghai, China), ROS assay kit, TUNEL assay kit, and cell counting kit 8 (CCK8) purchased from Shanghai Biyuntian Biological Co., LTD. The gel kit was purchased from Shanghai Yase Technology Biology Co., LTD. The agarose gel kit was purchased from Yisheng Biotechnology (Shanghai) Co., LTD. All chemical reagents were analytically pure unless otherwise stated.

Preparation of Ultrasonic Nanobubbles

Preparation of Different Nanobubbles

The solution injection method was used as follows: 2.3 mg DSPC and 0.7 mg DSPE-PEG were weighed and dissolved in a mixture of 300 μL ethanol and 100 μL tetrahydrofuran. A 2.7 mL of distilled water after the water film with pore size of 0.22 μm was used. The organic solution was slowly added to the vigorously stirred distilled water by syringe drip, and the organic solution was removed by dialysis to obtain the ultrasonic nanobubble empty nanobubble (NB). The obtained solution was freeze-dried and capped under vacuum. When the pressure in the bottle was negative, a syringe filled with perfluoropropane gas was inserted into the sealed penicillin bottle, and the bottle was filled with perfluoropropane gas. Carefully seal and store with sealing film.

CUR, DOX-CDM-PEG, or both were added to the organic solution to obtain curcumin-loaded nanobubbles (CNB), DOX-CDM-PEG loaded nanobubbles (DCNB), and dual-drug loaded nanobubbles (C/DCNB). DOX-CDM-PEG was replaced by DOX to obtain C/DNB. Rhodamine B and Indocyanine Green (ICG) were added to the organic solution to obtain nanobubbles with fluorescent indicator function.

Preparation of Acid-Sensitive Doxorubicin

A 1 mg of doxorubicin and 10 mg of CDM-PEG were dissolved in 1 mL of anhydrous DMF and stirred well at 0 °C. Next, 0.1 mg DMAP was added to the mixed solution and the reaction was allowed to take place for 24 h at room temperature. The resulting solution was dialyzed for 24 h, the water was changed once along the way, freeze-dried and stored at −20°C. CDM-PEG synthesis is described in the Item S1.

Characterization of Ultrasonic Nanobubbles

The hydrodynamic particle size and potential of ultrasonic nanobubbles were characterized by a dynamic light scatterometer (Nano ZS90, Malvern, UK). The nanobubbles were stored at 4°C and removed every other day to measure their characterization.

The morphology of ultrasonic nanobubbles was characterized by transmission electron microscopy (TEM, Hitachi HT7700), and electron microscope samples were prepared as follows: 10 μL of the sample was dropped onto the electrolens and left for 2 min. The excess liquid was sucked off with filter paper, and the phosphotungstic acid-negative staining solution (10 μL, 2%) was dropped again for negative staining. After standing for 2 min, the excess liquid was sucked off and dried in a vacuum drying oven overnight.

Ultrasound contrast-enhanced images of ultrasound nanobubbles were obtained using a Toshiba Canon Aplio 500 color ultrasound diagnostic instrument with a linear probe (5–12 MHz).

The UV–vis absorption spectrum was measured by u-3900 UV spectrophotometer. The absorbance values of different concentrations of drugs were measured by UV spectrophotometer to prepare the standard curve of drug concentration. After the nanobubbles were completely destroyed by ultrasound, the absorbance value of the free drug in the solution was measured to obtain the drug loading. The release of CUR and DOX was measured under different conditions by treating

the nanobubbles with or without ultrasound and adjusting the pH value of the PBS solution. Formula for calculating drug loading capacity in Table S1.

DOX-CDM-PEG, CDM-PEG, NB, CNB, DCNB, and C/DCNB were dispersed in DMSO-D_6, Chloroform-D or D_2O, and characterized by Proton nuclear magnetic resonance (^{1}H NMR) (AVANCEIII, Bruker, Switzerland).

Biocompatibility Testing

The mice were injected with 200 μL (200 μg/mL) nanobubbles solution and PBS solution every hour for 12 consecutive times. After observation for 7 days, the mice were sacrificed. Blood samples were collected for routine blood tests and blood biochemical tests. The heart, liver, spleen, lung and kidney were removed for Hematoxylin and Eosin (H&E) staining. The difference between the control group and the empty nanobubbles group was observed. At the same time, the body weight of mice was monitored every day.

In vitro Cytotoxicity

Mouse liver cancer cells line Hepa 1–6 and mouse normal liver cells line AML 12 were purchased from ATCC. Hepa 1–6 and AML 12 were seeded at a density of 5000 cells per well in 96-well plates and cultured for 24 h. Then, different nanobubbles of the same concentration were added and part of the groups were exposed to ultrasound (each group had 6 parallel Wells), and incubated together for 24 h and 48 h, respectively. The cell viability was detected by CCK8.

Hepa1-6 cells (5×10^4 cells per well) were spread on the 96-well plates for 24 h, and then the medium was replaced by medium containing different nanobubbles and cultured with or without ultrasound. After 24 h, the cells were finally treated with TUNEL assay kit, and the cell apoptosis was observed under a fluorescence microscope.

Cell Uptake Capacity of Ultrasound Nanobubbles

The cellular uptake of ultrasound nanobubbles was evaluated using laser fluorescence microscope and flow cytometry. Hepa 1–6 and AML 12 cells were cultured in DMEM containing 10% FBS, 1% penicillin-streptomycin. The specific protocol was as follows: first, Hepa 1–6 cells were cultured in 6-well plates (density: 5×10^4 cells per well, 37°C, 5% CO^2) for 24 h. Then, the original medium was replaced with C/DCNB (pH 7.4), C/DNB (pH 7.4) and C/DCNB (pH 6.8) for 6 h (all nanobubbles have been loaded with Rhodamine B). Adjusting pH of medium with lactic acid. The cells were then fixed with 4% paraformaldehyde and stained with DAPI. They were observed under a fluorescence microscope. Hepa1-6 cells (density: 3×10^6 cells per well) were plated in 6-well plates for 24 h and incubated with medium containing nanobubbles under the same conditions for 6 h. Finally, the cells were digested and resuspended in PBS solution and detected by flow cytometry.

Ultrasound-Activated ROS Generation

To assess intracellular ROS production, DCFH-DA fluorescent probe was used to detect ROS produced by ultrasound-activated sonosensitizer. Hepa1-6 cells were cultured at 3×10^5 cells per well in 6-well plates for 24 h, then the medium containing nanobubbles was replaced for 6 h, and then the medium containing nanobubbles was replaced by the medium containing DCFH-DA fluorescent probe. The cells were incubated in an incubator in the dark for 30 min and then digested and analyzed by flow cytometry.

Detection of Microbubble Contrast Imaging in vitro and vivo

For in vitro imaging evaluation, an agarose gel was prepared to simulate the in vivo environment of mice. The nanobubbles solution was injected into the pit of the gel, and the Toshiba Canon Aplio 500 color ultrasound diagnostic instrument was used to evaluate the contrast imaging of the nanobubbles solution in the hole. For in vivo imaging evaluation, the specific location of the subcutaneous tumor was first found by the probe, and the subcutaneous tumor was observed at the same time as the intravenous injection of the nanobubbles.

The nanobubbles were resuspended by injecting PBS solution with a syringe in the closed glass bottle, shaking vigorously, and then extract the nanobubble solution. Agarose gels were synthesized in Item S2.

In vivo Distribution

Female BALB/c mice (4–6 weeks) were used to establish Hepa1-6 subcutaneous hepatocellular carcinoma models. First, Hepa1-6 cells were digested and evenly dispersed in PBS solution. Then, 200μL of the cell suspension was subcutaneously injected into the abdomen of each mouse, and the mice were fed for 14 days to prepare for the next experiment. The tumor volume of mice was calculated as follows: tumor volume (V) = (length × width²) / 2. Where, the length is the longest dimension of the tumor, and the width is the shortest dimension of the tumor.

Fourteen days after subcutaneous implantation of tumors in mice, the mice were divided into four groups (n=3) and injected with 200 μL of ICG loaded C/DNB, C/DCNB, C/DCNB+US, and free ICG through the tail vein, respectively, followed by immediate tumor sonication or no treatment. ICG was used as a fluorescent dye to label the nanobubble, and the distribution of the nanobubbles in mice was observed. After 24 h, the mice were sacrificed, and the main organs (heart, liver, spleen, lung, kidney) and tumors of the mice were collected for fluorescence imaging. The distribution of nanobubbles in different organs was analyzed.

Evaluation of Tumor Treatment Efficacy

Hepa 1–6 tumor-bearing BALB/c mice were randomly divided into five groups (n=5): PBS group, CNB, DCNB, C/DCNB, C/DCNB+US, C/DNB and CUR+DOX. Each group was injected with 200 μL of drugs via tail vein. After drug injection, ultrasound irradiation (1.0 MHz, 50% duty cycle, 2W/cm^2, 1 min) was performed immediately and then again 8 hours later. Treatment was performed every two days. After different treatments, the weight and tumor volume of the mice were monitored every two days. After 14 days, the mice were sacrificed, and their tumors were collected. This protocol was approved by the Ethics Committee of Tianjin Medical University Cancer Institute and Hospital. Animal welfare and experimental procedures were carried out in accordance with the National Research Council's Guide for the use of laboratory animals.

Antitumor Mechanism Verification

Hepa 1–6 cells (5×10^4 cells per well) were spread in 6-well plates and incubated for 24 h to make the cells adhere to the wall, then the medium containing different nanobubbles was replaced and incubated with ultrasound or without ultrasound for 24 h, and the protein was extracted. Expression was examined after testing protein concentrations using the BCA kit.

Tumor cells were incubated with DCNB and C/DCNB, and flow cytometry was employed to quantify the intracellular doxorubicin content.

Statistical Analysis

The data are shown as the mean ± SD (standard deviation), and statistical analyses were performed using the Student's *t*-test (*p < 0.05, **p < 0.01, and ***p < 0.001).

Results and Discussion

Preparation and Characterization of Ultrasonic Nanobubbles

Nanobubbles were constructed by injecting organic solutions dissolved with DSPC, DSPE-PEG2000 and different drugs into the distilled water through the membrane with high speed stirring. Transmission electron microscopy results showed that nanobubbles with uniform size were successfully constructed, as shown in Figure 1B–E. The size of nanobubbles measured by transmission electron microscopy was about 100 nm-200 nm. Figure 1A shows the internal structure of various nanobubbles loaded with different drugs. The successful synthesis of acid-sensitive DOX and the success of drugs encapsulation in nanobubbles were proved by ^{1}H NMR spectroscopy. The ^{1}H NMR of DOX-CDM-PEG, CDM-PEG and various nanobubbles are shown in Figure S1. Figure 1F and G show the hydrated particle size and potential of the nanobubbles loaded with different drugs, respectively. The hydration particle sizes of NB, CNB, DCNB and C/DCNB were 162nm, 200.7nm, 163.6nm and 170.5nm, respectively. The results indicate that the C/DCNB had almost zero potential and were electrically neutral. We measured the hydration particle size, zeta potential, and polymer dispersity index (PDI) of C/DCNB at different time points

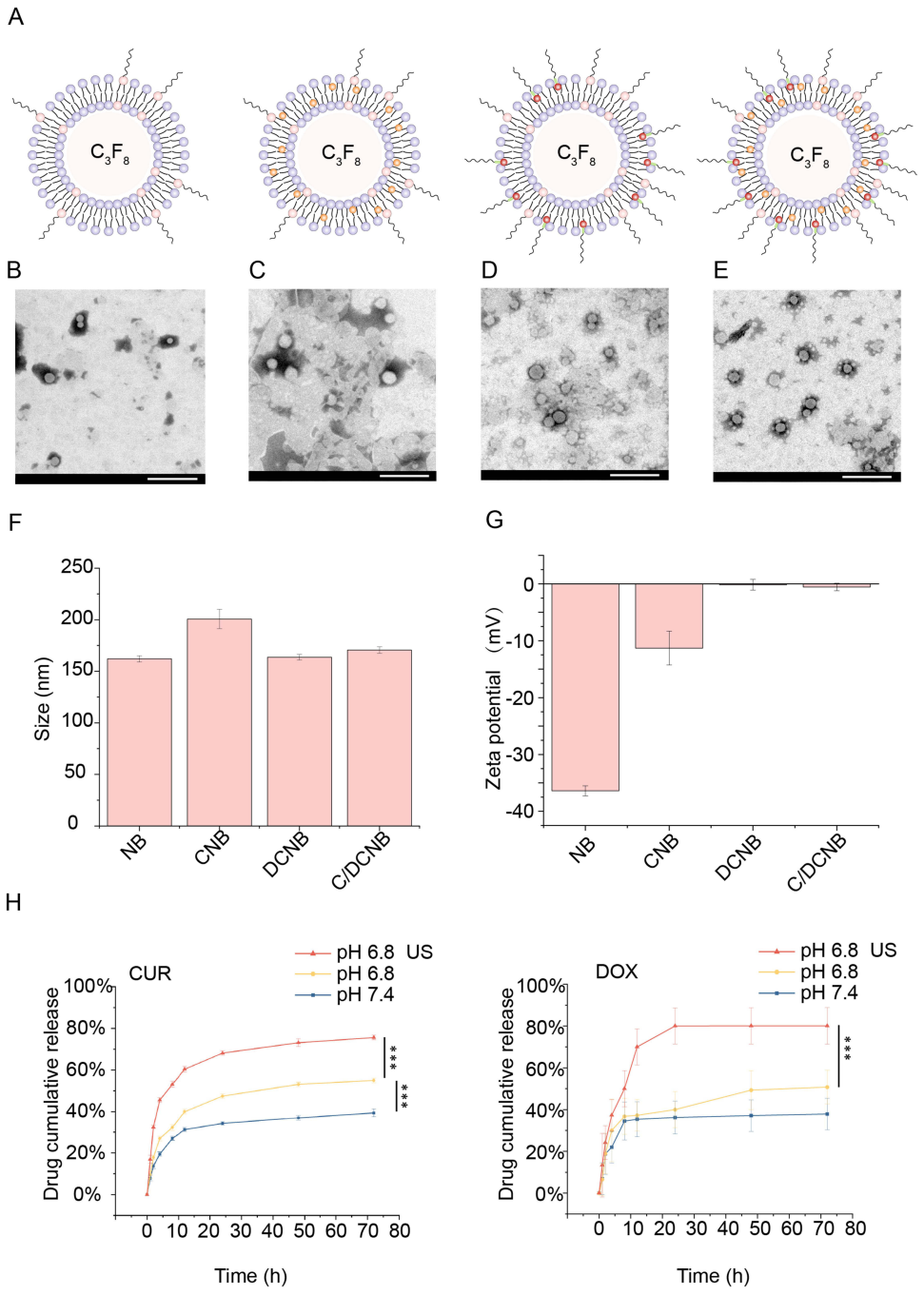

Figure 1 (**A**) Schematic diagram of structure of nanobubbles, The yellow ball is curcumin, the red ball is doxorubicin. (**B**) TEM images of the NB. (**C**) TEM images of the CNB. (**D**) TEM images of the DCNB. (**E**) TEM images of the C/DCNB. (**F**) Histogram of the hydrated particle size of the nanobubbles. (**G**) Potential histogram of nanobubbles. (**H**) The cumulative release rates of CUR and DOX over 3 days. Scale bar = 500 nm. ***P < 0.001 (Student's *t*-test).

during a week in Figure S2. These parameters did not show significant changes over time, and the PDI value remained consistently below 0.35. These result conclude that the nanobubble exhibits good stability in aqueous solution. This stability may be attributed to the bulky hydrophilic PEG headgroup pointing into the continuous media.[27] These parameters are important physicochemical properties that affect cellular endocytosis and the efficiency of endocytosis. The distribution of nanoliposomes with a particle size of 100 nm-200 nm in tumor tissue is higher than that of nanoliposomes with a particle size of over 300 nm or below 50 nm.[28], 200 nm is the internalization mediated by the gradual transition of cell endocytosis from

clathrin-dependent to caveolae-mediated.[29] The internalization efficiency of particles smaller than 200 nm is relatively high. In summary, we have successfully prepared electrically neutral liposomal nanobubbles with particle size of about 100 nm-200 nm.

Drug Release and Drug Loading Capacity

The drug loading capacity of CUR and DOX is shown in Table S1. The release of CUR and DOX is shown in Figure 1H. In the absence of ultrasound at pH 7.4, the C/DCNB degraded slowly and the maximum release rate is about 40%. After adjusting the pH of the release environment to 6.8, the release speed and release amount are increased, and the maximum can reach almost 50%. The results indicate that the shedding of CDM-PEG facilitates drug release. The drug release is relatively slow under the conditions of pH 7.4 and 6.8 without ultrasound, and there is a significant release only after the irradiation of ultrasound. The maximum release of CUR and DOX reached 73.12% and 80% at 48 h. Ultrasound indeed plays a crucial role in facilitating the release of drugs from nanobubbles.

Biocompatibility of NB and Cytotoxicity of Nanobubbles

To validate the biocompatibility of the nanobubbles, the cytotoxicity of the nanobubbles on AML 12 was measured. As shown in Figure 2B, the cell viability of AML 12 was close to 100% after 24 hours of co-incubation with empty nanobubbles, and the

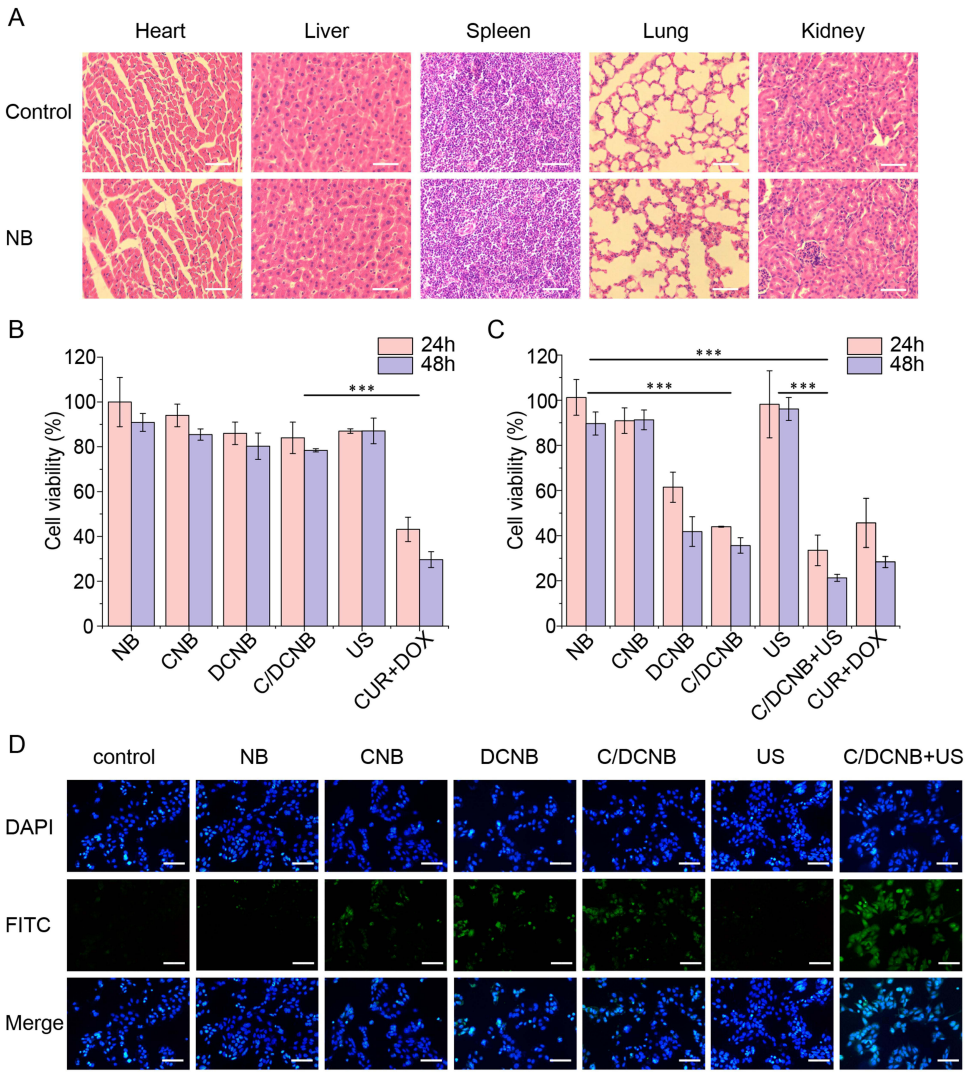

Figure 2 (**A**) H&E assay of the major organ in BALB/c mice after injection of NB (24 mg·kg^{-1}) via the tail vein. (**B**) Cell viability of NB, CNB, DCNB, C/DCNB, US and CUR +DOX in AML 12 cells at 24 h and 48 h. (**C**) Cell viability of NB, CNB, DCNB, C/DCNB, US, C/DCNB+US and CUR+DOX in Hepa 1–6 cells at 24 h and 48 h. (**D**) TUNEL staining analysis, green fluorescence represents apoptosis situation. Scale bar = 50 μm. ***P < 0.001 (Student's *t*-test).

cell viability decreased slightly but was still above 90% after 48 hours. The results show that empty nanobubbles had no significant cytotoxic effect on AML 12 cells. The cell viability of the drug-loaded nanobubbles in AML 12 cells was more than 80%. Due to CDM-PEG does not peel off at pH 7.4, an increased density of PEG on the carriers' surface would affect the endocytosis of nanobubbles by AML 12 cells.[30] To further prove the role of nanobubble in reducing toxicity to normal cells, we examined the cytotoxicity of free drugs on AML 12. The cell viability of AML 12 at 24 h and 48 h were 43% and 29%, respectively. The free drug group had a significant cytotoxicity effect on AML 12 cells compared with the C/DCNB group, further demonstrating the protective effect of the nanobubbles on normal cells.

The results of acute toxicity test in mice are shown in Figure 2A. The empty nanobubbles were injected into BALB/c mice to reach 24 $mg \cdot kg^{-1}$ within 12 h through the tail vein. After 14 days, all the mice survived without significant weight loss, and we observed no deaths or behavioral abnormalities during the treatment. After the mice were sacrificed, the organs were taken for H&E staining, and there was no obvious inflammatory infiltration. There are also no differences between the empty nanobubbles and control groups. In addition, we also tested the biochemical indicators and blood routine of the control group and the NB group in Figure S3. The measured values were found to be within the normal range, and there was no significant difference observed between the values of the NB group and the control group. Both in vitro and vivo experiments have consistently shown that empty nanobubbles exhibit excellent biocompatibility.

To study the anti-tumor ability of C/DCNB, we evaluated the anti-tumor effect of nanobubbles in vitro, as shown in Figure 2C. The cell viability of the NB group and the ultrasound group were both higher than 90%, indicating that the empty nanobubbles and ultrasound had no obvious toxic effect on the cells. Both the C/DCNB and C/DCNB+US groups exhibited statistically significant differences compared to the NB group, indicating that the combination of CUR and DOX exhibit positive anti-tumor effects. The cytotoxicity effect of C/DCNB+US group on tumor cells was stronger than that of C/DCNB group, and there was a significant statistical difference between C/DCNB+US and US group. These results demonstrate that ultrasound alone lacks cytotoxicity, and C/DCNB exhibited an enhanced anti-tumor effect under ultrasound condition. These results show that C/DCNB combined with ultrasound had a better therapeutic effect on Hepa1-6 cells in vitro.

To further verify the anti-tumor ability of C/DCNB. The TUNEL assay kit was employed to assess the anti-tumor capability of nanobubbles. There was basically no green fluorescence in the empty nanobubbles group and the ultrasound group in Figure 2D, which further confirmed that the NB and US had no cytotoxicity on Hepa1-6 cells. The intensity of green fluorescence observed in the C/DCNB+US group was significantly higher than that in the C/DCNB group. This result is consistent with the cytotoxicity results, indicating that ultrasound can effectively enhance the anti-tumor effect of C/DCNB by exposing CUR to ultrasound conditions. The above results demonstrate that C/DCNB combined with ultrasound has great anti-tumor ability and reduced toxic side effects on normal cells.

Cellular Uptake

To verify the endocytosis of C/DCNB, the medium was adjusted to be acidic to simulate the tumor microenvironment. As shown in Figure 3A by fluorescence microscopy, C/DCNB showed a positive endocytosis effect at pH 6.8. This was attributed to the peeling off CDM-PEG in the acidic environment, leading to a reduction in PEG on the surface of the nanobubbles and facilitating the endocytosis of the nanobubbles by the cells. C/DNB also showed good endocytosis at pH 7.4. However, the fluorescence effect of C/DCNB co-cultured with cells at pH 7.4 was much lower than that of the above two groups, because excessive surface PEG is adverse to the endocytosis of nanobubbles by cells.[30]

The results of flow cytometry, as shown in Figure 3B, showed that the fluorescence intensity of Hepa1-6 cells incubated with C/DCNB at pH 6.8 was similar to that of Hepa1-6 cells incubated with C/DNB at pH 7.4, and both were higher than that of Hepa1-6 cells incubated with C/DCNB at pH 7.4. These results indicate that the nanobubbles peeled off by CDM-PEG in acidic environments enhance the endocytosis ability of cancer cells.

ROS Generation

The flow cytometry results of ROS produced by sonosensitizer are shown in Figure 3C. The sonosensitizer CUR produces ROS under ultrasound conditions, which can oxidize the probe in the kit to produce fluorescent substances. And

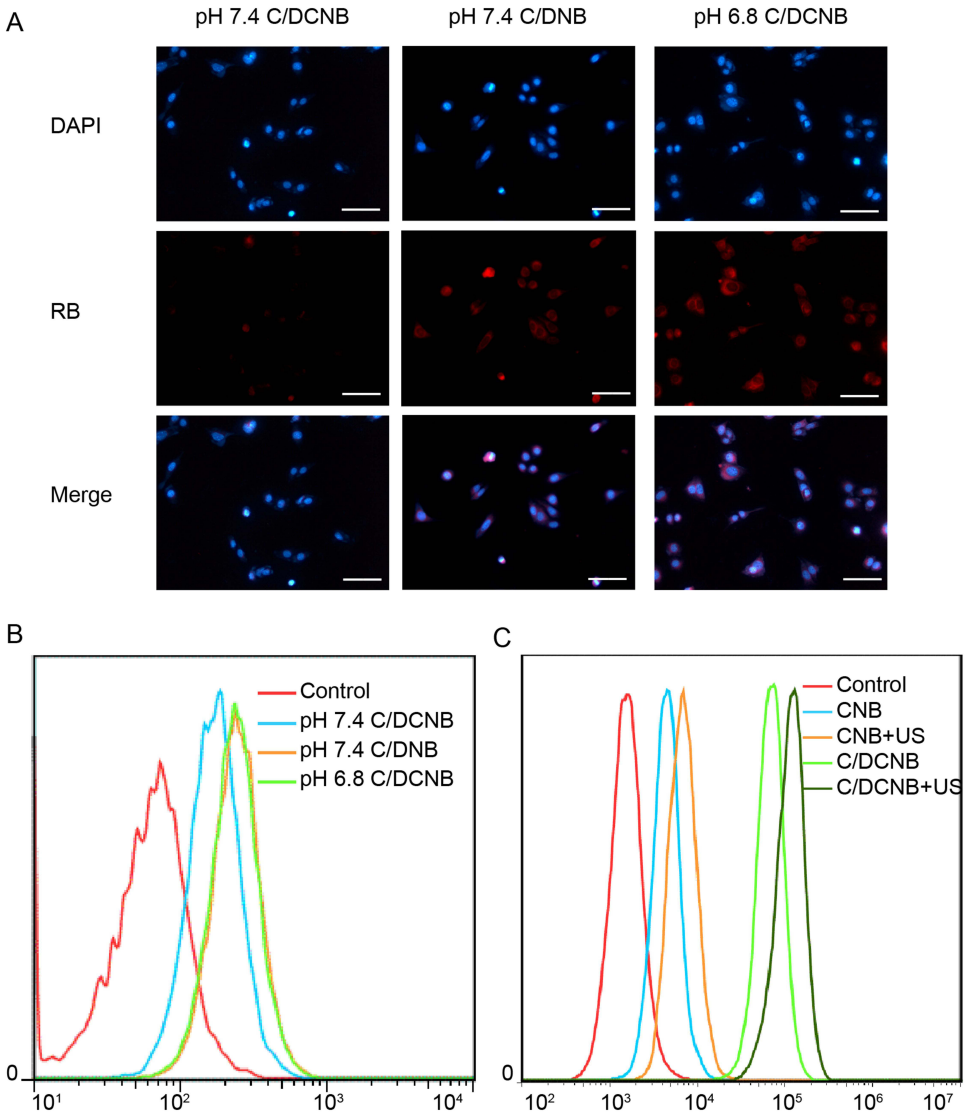

Figure 3 (**A**) Images of in vitro cellular uptakes of different fluorescence-decorated nanobubbles characterized by fluorescence microscopy. (**B**) Flow cytometry results of Hepa1-6 cells after treated with nanobubbles. (**C**) Flow cytometry the results of ROS production by sonosensitizers in Hepa1-6 cells. Scale bar = 100 μm.

the fluorescence intensity is positively correlated with the level of ROS in the cells. Flow cytometry results show that higher fluorescence intensity was observed in the C/DCNB group and CNB group under ultrasonic conditions compared to the C/DCNB group and CNB group without ultrasonic conditions. These results prove that ultrasound irradiation could induce the production of ROS.

In vitro Ultrasound Imaging of C/DCNB

To investigate the ultrasound imaging ability of C/DCNB as an ultrasound contrast agent, a gel model was used to simulate tissue blood vessels to observe the CEUS signal after C/DCNB injection. As shown in Figure 4A, the ultrasound contrast signal was almost invisible in the control group, while there was a significant enhancement signal in the C/DCNB group. Indicating a good ultrasound contrast capability of C/DCNB. The signal was present for more than 3 minutes. The quantitative gray values of the C/DCNB group exhibit significant increases compared to the control (Figure 4B).

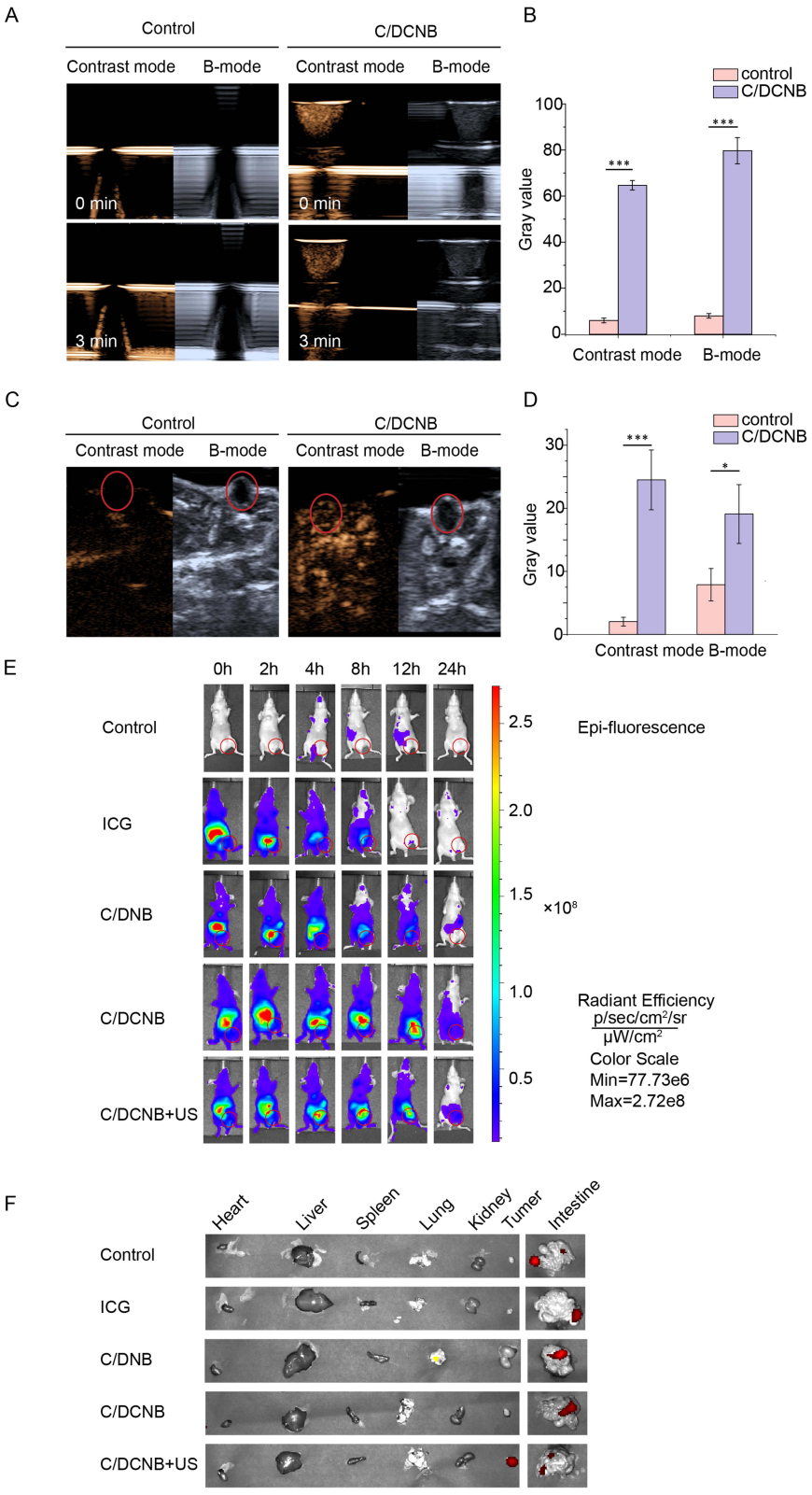

Figure 4 Evaluation of (**A**) in vitro and (**C**) in vivo contrast imaging of nanobubbles using clinical ultrasound systems. The gray value of the ultrasound images in the presence or absence of C/DCNB (**B**) in vitro and (**D**) in vivo. (**E**) In vivo distribution of Hepa 1–6 tumor-bearing mice during 24 h. Red circle indicates the tumor location. (**F**) Fluorescence images of major organs and tumors of mice at 24 h.*P < 0.05, ***P < 0.001 (Student's *t*-test).

In vivo US Imaging, Fluorescence Imaging

The in vivo CEUS imaging results of the nanobubbles are shown in Figure 4C. C/DCNB showed great ultrasound imaging capability in vitro, we observed its imaging effect in mice after tail vein injection of C/DCNB. The imaging efficacy of C/DCNB in subcutaneous mice tumors is depicted. Employing a clinical imaging system for subcutaneous tumor detection, the pre-injection phase revealed a virtually negligible signal within the tumor. However, following injection, the ultrasound imaging signal peaked at its maximum intensity within 30 seconds. It is proved that C/DCNB has excellent US imaging capability. The quantitative gray values of the tumor tissues exhibit significant increases compared to the non-treated mice (Figure 4D).

The distribution of nanobubbles after different treatments in mice is shown in Figure 4C. Initially, the fluorescence was distributed throughout the body in mice, gradually accumulating at the tumor site over time. After 24 hours, the main organs and tumors were dissected out. As shown in Figure 4E, obvious fluorescence was found in the C/DCNB+US group, indicating that local ultrasound irradiation can promote the accumulation of drugs in the tumor site. The reason may be explained by the combination of ultrasound and C/DCNB enhancing the penetration of the tumor vascular membrane and the entry of C/DCNB into the tumor tissue.[20] The fluorescence signal in the ICG group had basically disappeared at 12 hours, and the fluorescence signal in the C/DCNB group and the C/DCNB+US group still had fluorescence signal at 24 hours. There was no obvious fluorescence in the tumor site of the C/DNB group at 24 hours. The reason is that the modified PEG on the surface of C/DCNB reduces the reticuloendothelial system (RES) clearance ability.[3] The C/DCNB group in Figure 4C also had a tendency to gradually reach the tumor site. However, there was no significant fluorescence observed in the in ex vivo tumor tissue, while fluorescence was detected in the small intestine of the C/DCNB group in Figure 4F. The main reason for this result that, in comparison to C/DCNB+US, C/DCNB exhibit fewer accumulation at the tumor site and metabolism from the small intestine. Overall, in vivo distribution studies, demonstrating that the combination of C/DCNB and ultrasound enhances drug accumulation in tumors. ICG-loaded nanobubbles are characterized in Figure S4.

Anti-Tumor Effects of Nanobubbles

Considering that the combination of ultrasound with C/DCNB could enhance drug delivery to the tumor, the in vivo anti-tumor efficacy was further investigated. The average initial volume of the tumor was about 50 mm^3. The tumor was treated with PBS, CNB, DCNB, C/DCNB, C/DCNB+US, C/DNB and CUR+DOX, and the tumor volume and body weight of the mice were observed. Tumor volume and body weight as shown in Figure 5A and B. Both C/DCNB+US and C/DCNB groups show statistically significant differences from the control group, and the results indicate that C/DCNB had good anti-tumor ability. The significant statistical difference between C/DNB and C/DCNB further demonstrate that the surface modified PEG of C/DCNB reduced the clearance ability of reticuloendothelial system (RES)[31] and enhanced drug accumulation in tumors. A significant statistical difference between C/DCNB+US and C/DCNB further confirmed that ultrasound stimulation effectively enhances the anti-tumor capability of C/DCNB. The findings indicate that ultrasound facilitated the accumulation of C/DCNB at the tumor site, which is consistent with the results of fluorescence distribution in mice. When C/DCNB accumulate at the tumor site and irradiated by ultrasound, ultrasound facilitates the release of drugs and activate sonosensitizers, leading to the generation of ROS. This process ultimately triggers apoptosis in tumor cells, highlighting the potential of this approach as an effective anti-tumor strategy.

The tumor volume of C/DCNB was smaller than those of the two groups of single-drug nanobubbles CNB and DCNB, due to CUR could inhibit the expression of P-glycoprotein (P-gp) and reduce the drug resistance of tumor cells to DOX. No significant body weight loss was observed during the treatment, indicating that these different treatments did not cause significant toxic effects on the mice. To further examine the contribution of nanobubbles to enhancing therapeutic efficacy and reducing systemic toxic effects. We establish the free drug group to observe the tumor changes and the body weight of mice. As shown in Figure 5B, the free drug group show a rapid decrease in body weight owing to the side effects of free-induced acute toxicity, and free drug only moderately inhibit tumor growth compared with the control group. The results of P-gp, cytochrome C (Cyt C) and caspase3 staining analysis can verify the specific anti-tumor mechanism of C/DCNB in vivo; C/DCNB decreased the expression of P-gp and increased the expression of cytochrome C and caspase3 in the tumor (Figure 5E). The changes in tumor volume showed that C/DCNB + US can inhibit the proliferation of tumor cells, and its inhibitory ability was significantly higher than that of the other groups. After 14 days of treatment, the mice were sacrificed, and the subcutaneous tumor volume is shown in Figure 5D.

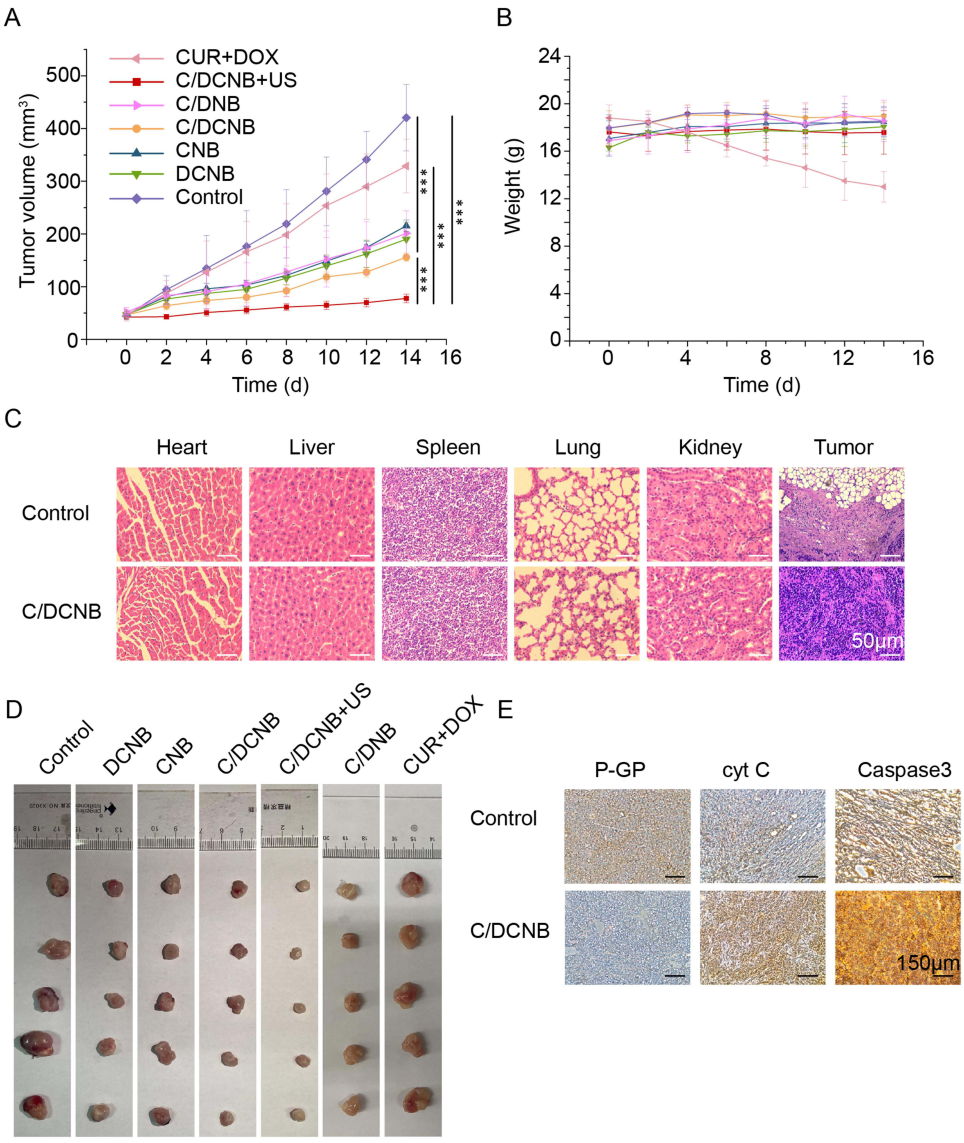

Figure 5 (**A**) tumor volumes and (**B**) the body weights of tumor-bearing BALB/c mice during treatment. (**C**) H&E staining of the major organ and tumor tissue slices. Scale bar = 50 μm. (**D**) Solid tumors after 14 days of administration in control, CNB, DCNB, C/DCNB, C/DCNB+US, C/DNB and CUR+DOX groups. (**E**) Immunohistochemical staining of tumor slices. Scale bar = 150 μm. ***P < 0.001 (Student's *t*-test).

Antitumor Mechanisms

The anti-tumor mechanisms of CUR and DOX were analyzed by Western blot. Results as shown in Figure 6A, the expression of P-gp in CNB, C/DCNB, C/DCNB+US was significantly lower than that in the control group, indicating that CUR had a significant inhibitory effect on P-gp of tumor cells. We measured the content of doxorubicin in C/DCNB and DCNB tumor cells by flow cytometry. As shown in Figure 6B, the content of doxorubicin in C/DCNB group was stronger than that in DCNB group, which further prove that C/DCNB reduced the resistance of tumor cells to doxorubicin.

The highest protein expression levels of cytochrome C (Cyt C) and caspase3 in the C/DCNB+US group may be the reason for the up-regulation of Cyt C expression caused by internalization of CUR and DOX.[32–34] This change prompts Cyt C to form apoptotic bodies, subsequently activating caspase-3 and initiating the caspase cascade.[35] These findings were corroborated by Western blot analysis, providing compelling evidence of the apoptotic pathway activation induced by the synergistic action of CUR and DOX encapsulated in the nanobubbles, further potentiated by ultrasound stimulation. Meanwhile, CUR produces ROS under ultrasound stimulation. ROS leads to a reduction in mitochondrial membrane potential, causing an increase in the permeability of the mitochondrial inner membrane. Consequently,

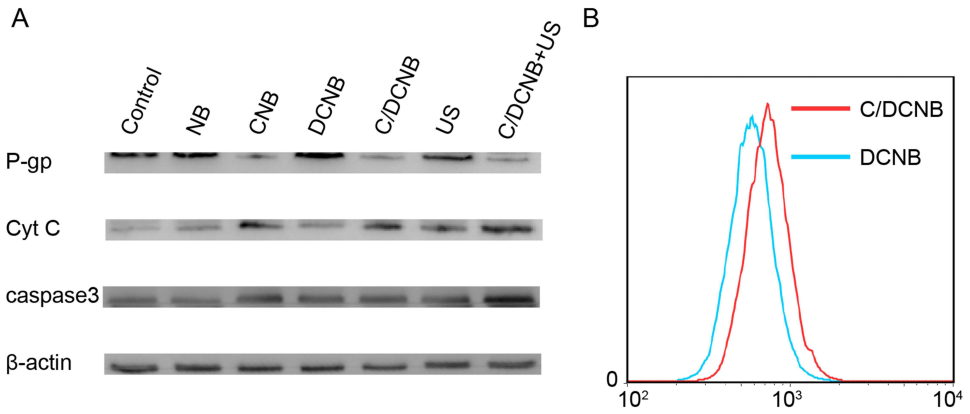

Figure 6 (**A**) Expression of p-glycoprotein, cytochrome C, caspase3 in Hepa 1–6 cells treated with nanobubbles for 24 hours. (**B**) Flow cytometry results of intracellular doxorubicin content in hepa 1–6 cells.

cytochrome C is released from the mitochondria.[36–38] This phenomenon results in higher protein expression levels of cytochrome C and caspase3 in the C/DCNB+US group compared to the C/DCNB group.

Both CUR and DOX could up-regulate the expression of Cyt C, and CUR inhibits the expression of P-gp to increase the accumulation of DOX. Therefore, as shown in Figure 5E, the expression of Cyt C and caspase3 in C/DCNB group was higher than that in CNB and DCNB groups, suggesting that the synergistic treatment effect of two drugs is better than that of single drug. These results prove that the effect of sonodynamic assisted dual drug synergistic therapy is considerable.

Conclusion

The study focused on developing nanoscale CUR-DOX loaded nanobubbles C/DCNB specifically designed to respond to the tumor microenvironment and reduce normal tissue toxicity. C/DCNB exhibited excellent biocompatibility and mitigated the adverse effects typically associated with direct chemotherapy. C/DCNB has a synergistic effect and can significantly improve the treatment efficiency on HCC. The inclusion of CUR inhibited P-gp expression in tumor cells, leading to increased DOX accumulation and promoted tumor cell apoptosis. Under ultrasound condition, the generation of ROS contributed to the apoptosis of tumor cells. The nanoscale nature of C/DCNB enables enhanced penetration into the tumor microenvironment. Experimental results suggest that C/DCNB holds promise as a potential treatment for HCC.

Acknowledgments

Xi Wei is the first corresponding author and Xiujun Gao is the second correspondence author for this study. This work was supported by the National Natural Science Foundation of China (No. 82272008). Funded by Tianjin Key Medical Discipline (Specialty) Construction Project (TJYXZDXK-009A).

Disclosure

The authors declare no conflicts of interest in this work.

References

1. Anwanwan D, Singh SK, Singh S, Saikam V, Singh R. Challenges in liver cancer and possible treatment approaches. *Biochim Biophys Acta Rev Cancer*. 2020;1873(1):188314. doi:10.1016/j.bbcan.2019.188314
2. Llovet JM, Kelley RK, Villanueva A, et al. Hepatocellular carcinoma. *Nat Rev Dis Primers*. 2021;7(1):6. doi:10.1038/s41572-020-00240-3
3. Shi Y, Wang J, Huang G, et al. A novel epithelial-mesenchymal transition gene signature for the immune status and prognosis of hepatocellular carcinoma. *Hepatol Int*. 2022;16(4):906–917. doi:10.1007/s12072-022-10354-3
4. Kong FH, Ye QF, Miao XY, et al. Current status of sorafenib nanoparticle delivery systems in the treatment of hepatocellular carcinoma. *Theranostics*. 2021;11(11):5464–5490. doi:10.7150/thno.54822
5. Gao X, Bao K, Zhang Y, et al. The synergistic effects of multidrug-loaded nanocarriers improve tumor microenvironment responsive chemo-sonodynamic therapy of hepatocellular carcinoma. *Adv Funct Mater*. 2023;33(29):1.
6. Wu T, Liu Y, Cao Y, Liu Z. Engineering macrophage exosome disguised biodegradable nanoplatform for enhanced sonodynamic therapy of glioblastoma. *Adv Mater*. 2022;34(15):e2110364. doi:10.1002/adma.202110364

7. Qian X, Zheng Y, Chen Y. Micro/nanoparticle-augmented sonodynamic therapy (SDT): breaking the depth shallow of photoactivation. *Adv Mater*. 2016;28(37):8097–8129. doi:10.1002/adma.201602012
8. Zhang Y, Zhang X, Yang H, et al. Advanced biotechnology-assisted precise sonodynamic therapy. *Chem Soc Rev*. 2021;50(20):11227–11248. doi:10.1039/D1CS00403D
9. Ryu JH, Yoon HY, Sun IC, Kwon IC, Kim K. Tumor-targeting glycol chitosan nanoparticles for cancer heterogeneity. *Adv Mater*. 2020;32(51): e2002197. doi:10.1002/adma.202002197
10. Xu M, Zhou L, Zheng L, et al. Sonodynamic therapy-derived multimodal synergistic cancer therapy. *Cancer Lett*. 2021;497:229–242. doi:10.1016/j.canlet.2020.10.037
11. Liang S, Deng X, Ma P, Cheng Z, Lin J. Recent advances in nanomaterial-assisted combinational sonodynamic cancer therapy. *Adv Mater*. 2020;32 (47):2003214. doi:10.1002/adma.202003214
12. Tian Y, Liu Y, Wang L, et al. Gadolinium-doped hollow silica nanospheres loaded with curcumin for magnetic resonance imaging-guided synergistic cancer sonodynamic-chemotherapy. *Mater Sci Eng C Mater Biol Appl*. 2021;126:112157. doi:10.1016/j.msec.2021.112157
13. Mattioli R, Ilari A, Colotti B, Mosca L, Fazi F, Colotti G. Doxorubicin and other anthracyclines in cancers: activity, chemoresistance and its overcoming. *Mol Aspects Med*. 2023;93:101205. doi:10.1016/j.mam.2023.101205
14. Lin L, Fan Y, Gao F, et al. UTMD-promoted co-delivery of gemcitabine and miR-21 inhibitor by dendrimer-entrapped gold nanoparticles for pancreatic cancer therapy. *Theranostics*. 2018;8(7):1923–1939. doi:10.7150/thno.22834
15. Feng T, Wei Y, Lee RJ, Zhao L. Liposomal curcumin and its application in cancer. *Int J Nanomed*. 2017;12:6027–6044. doi:10.2147/IJN.S132434
16. Son S, Kim JH, Wang X, et al. Multifunctional sonosensitizers in sonodynamic cancer therapy. *Chem Soc Rev*. 2020;49(11):3244–3261. doi:10.1039/C9CS00648F
17. Tang H, Zheng Y, Chen Y. Materials Chemistry of Nanoultrasonic Biomedicine. *Adv Mater*. 2017;29(10). doi:10.1002/adma.201604105
18. Ma J, Xu CS, Gao F, Chen M, Li F, Du LF. Diagnostic and therapeutic research on ultrasound microbubble/nanobubble contrast agents (Review). *Mol Med Rep*. 2015;12(3):4022–4028. doi:10.3892/mmr.2015.3941
19. Sirsi SR, Borden MA. Advances in ultrasound mediated gene therapy using microbubble contrast agents. *Theranostics*. 2012;2(12):1208–1222. doi:10.7150/thno.4306
20. Duan L, Yang L, Jin J, et al. Micro/nano-bubble-assisted ultrasound to enhance the EPR effect and potential theranostic applications. *Theranostics*. 2020;10(2):462–483. doi:10.7150/thno.37593
21. Kong X, Qi Y, Wang X, et al. Nanoparticle drug delivery systems and their applications as targeted therapies for triple negative breast cancer. *Prog Mater Sci*. 2023;134:101070.
22. Liu K, Huang L, Qi S, et al. Ferroptosis: the entanglement between traditional drugs and nanodrugs in tumor therapy. *Adv Healthc Mater*. 2023;12 (12):2203085. doi:10.1002/adhm.202203085
23. Singleton DC, Macann A, Wilson WR. Therapeutic targeting of the hypoxic tumour microenvironment. *Nat Rev Clin Oncol*. 2021;18(12):751–772. doi:10.1038/s41571-021-00539-4
24. He R, Zang J, Zhao Y, et al. Nanofactory for metabolic and chemodynamic therapy: pro-tumor lactate trapping and anti-tumor ROS transition. *J Nanobiotechnology*. 2021;19(1):426. doi:10.1186/s12951-021-01169-9
25. Sun H, Zhang Y, Zhong Z. Reduction-sensitive polymeric nanomedicines: an emerging multifunctional platform for targeted cancer therapy. *Adv Drug Deliv Rev*. 2018;132:16–32. doi:10.1016/j.addr.2018.05.007
26. Dacoba TG, Anthiya S, Berrecoso G, et al. Nano-oncologicals: a tortoise trail reaching new avenues. *Adv Funct Mater*. 2021;31(44):2009860. doi:10.1002/adfm.202009860
27. Chen M, Liang X, Gao C, et al. Ultrasound triggered conversion of porphyrin/camptothecin-fluoroxyuridine triad microbubbles into nanoparticles overcomes multidrug resistance in colorectal cancer. *ACS Nano*. 2018;12(7):7312–7326. doi:10.1021/acsnano.8b03674
28. Zhang M, Gao S, Yang D, et al. Influencing factors and strategies of enhancing nanoparticles into tumors in vivo. *Acta Pharm Sin B*. 2021;11 (8):2265–2285. doi:10.1016/j.apsb.2021.03.033
29. Saha K, Kim ST, Yan B, et al. Surface functionality of nanoparticles determines cellular uptake mechanisms in mammalian cells. *Small*. 2013;9 (2):300–305. doi:10.1002/smll.201201129
30. Oh N, Park JH. Endocytosis and exocytosis of nanoparticles in mammalian cells. *Int J Nanomed*. 2014;9(1):51–63. doi:10.2147/IJN.S26592
31. Gao X, Zhang J, He Z, et al. Targeting delivery of synergistic dual drugs with elastic PEG-modified multi-functional nanoparticles for hepatocellular carcinoma therapy. *Int J Pharm*. 2022;616:121567. doi:10.1016/j.ijpharm.2022.121567
32. Zhang Y, Liu S, Ma JL, et al. Apocynum venetum leaf extract alleviated doxorubicin-induced cardiotoxicity through the AKT/Bcl-2 signaling pathway. *Phytomedicine*. 2022;94:153815. doi:10.1016/j.phymed.2021.153815
33. Lu J, Li J, Hu Y, et al. Chrysophanol protects against doxorubicin-induced cardiotoxicity by suppressing cellular PARylation. *Acta Pharm Sin B*. 2019;9(4):782–793. doi:10.1016/j.apsb.2018.10.008
34. Pan MH, Chang WL, Lin-Shiau SY, Ho CT, Lin JK. Induction of apoptosis by garcinol and curcumin through cytochrome c release and activation of caspases in human leukemia HL-60 cells. *J Agric Food Chem*. 2001;49(3):1464–1474. doi:10.1021/jf001129v
35. Santucci R, Sinibaldi F, Cozza P, Polticelli F, Fiorucci L. Cytochrome c: an extreme multifunctional protein with a key role in cell fate. *Int J Biol Macromol*. 2019;136:1237–1246. doi:10.1016/j.ijbiomac.2019.06.180
36. Woo JH, Kim YH, Choi YJ, et al. Molecular mechanisms of curcumin-induced cytotoxicity: induction of apoptosis through generation of reactive oxygen species, down-regulation of Bcl-XL and IAP, the release of cytochrome c and inhibition of Akt. *Carcinogenesis*. 2003;24(7):1199–1208. doi:10.1093/carcin/bgg082
37. Zaccagnino P, Saltarella M, D'Oria S, Corcelli A, Saponetti MS, Lorusso M. N-arachidonylglycine causes ROS production and cytochrome c release in liver mitochondria. *Free Radic Biol Med*. 2009;47(5):585–592. doi:10.1016/j.freeradbiomed.2009.05.038
38. Che Y, Tian Y, Chen R, Xia L, Liu F, Su Z. IL-22 ameliorated cardiomyocyte apoptosis in cardiac ischemia/reperfusion injury by blocking mitochondrial membrane potential decrease, inhibiting ROS and cytochrome C. *Biochim Biophys Acta Mol Basis Dis*. 2021;1867(9):166171. doi:10.1016/j.bbadis.2021.166171